Microchimica Acta (2021) 188: 429
https://doi.org/10.1007/s00604-021-05097-1

ORIGINAL PAPER

Time-resolved fluorescence determination of albumin using ZnGeO:Mn luminescence nanorods modified with polydopamine nanoparticles

Lifang Gao[1] · Xu Zhang[1] · Runlin Yang[1] · Zhongwei Lv[2] · Wenge Yang[3] · Yonghong Hu[3] · Bin Zhou[1,4]

Received: 11 September 2021 / Accepted: 9 November 2021 / Published online: 24 November 2021
© The Author(s), under exclusive licence to Springer-Verlag GmbH Austria, part of Springer Nature 2021

Abstract

A novel time-resolved fluorescence (TRF) pobe is constructed to detect human serum albumin (HSA) by exploiting ZnGeO:Mn persistent luminescence nanorods (ZnGeO:Mn PLNRs) and polydopamine nanoparticles (PDA NPs). HSA-induced dynamic quenching leads to the fluorescence decrease of ZnGeO:Mn PLNRs, providing the basis for quantitative analysis of HSA. The excellent photo-thermal conversion performance of PDA NPs is helpful to the collision process between ZnGeO:Mn PLNRs and HSA, inducing significant improvement of sensitivity. HSA is quantified by measuring time-resolved fluorescence at 540 nm under excitation of 250-nm light. Under optimal conditions, HSA in the linear range 0.1–100 ng mL^{-1} are detected by this PDA-mediated ZnGeO:Mn probe with high sensitivity and selectivity, and the detection limit is 36 pg mL^{-1} ($3\sigma/s$). The RSD for the quantification of HSA (5 ng mL^{-1}, $n = 11$) is 5.2%. The practicability of this TRF probe is confirmed by accurate monitoring HSA contents in urine samples, giving rise to satisfactory spiking recoveries of 96.2–106.0%.

Keywords Persistent luminescence nanorods · Time-resolved fluorescence probe · Human serum albumin

Introduction

Human serum albumin (HSA) is one of the most important proteins in the human body, attributing to the momentous role in adjusting osmotic pressure of plasma, disposing of exogenous ligands and transporting substances of circulatory system [1–3]. A normal amount of HSA in urine is less than 30 mg L^{-1} and excess HSA level is closely related to a series of diseases, such as micro-/macro-albuminuria, cardiovascular disease, diabetes mellitus, and progressive glomerular failure of kidneys [4–6]. It is extremely necessary to detect albumin in urine, due to its important role in diagnosis and prevention medicine. The determination of HSA have attracted much attention of scientists, and varieties of methods have been adopted, including capillary electrophoresis, surface-enhanced Raman scattering spectroscopy (SERS), absorption spectrophotometry, and fluorescence techniques [7–10]. The capillary electrophoresis exhibits poor preparation ability, SERS usually requires expensive instruments, and absorption spectrophotometry has low sensitivity. Among them, fluorescence analysis techniques have been gaining increasing interest and widely applying to sensing and imaging. However, the components of urine samples are complex, which contains numerous proteins, nucleic acids, small molecules, and inorganic salt. The auto-fluorescence and scattering light of these components give rise to high background noise, causing a limited sensitivity and accuracy [11, 12].

Lifang Gao and Xu Zhanghave equally contributed to this work.

✉ Lifang Gao
gaolifang@jsinm.org

✉ Bin Zhou
zhoubin@jsinm.org

[1] NHC Key Laboratory of Nuclear Medicine, Jiangsu Key Laboratory of Molecular Nuclear Medicine, Jiangsu Institute of Nuclear Medicine, Wuxi 214063, Jiangsu, China

[2] Department of Nuclear Medicine, Shanghai 10Th People's Hospital, Tongji University School of Medicine, Shanghai 200000, China

[3] The Synergetic Innovation Center for Advanced Materials, State Key Laboratory of Materials-Oriented Chemical Engineering, College of Biotechnology and Pharmaceutical Engineering, Nanjing Tech University, Nanjing 211816, China

[4] Department of Radiopharmaceuticals, School of Pharmacy, Nanjing Medical University, Nanjing 211166, Jiangsu, China

In this regard, time-resolved fluorescence (TRF) analysis can effectively eliminate interference of autofluorescence and scattering light by using the long-lived luminescent materials and setting up a delay time of fluorescence collection. The lifetime of long-lived luminescent materials are longer than short-lived autofluorescence and the signals of long-lived materials can be collected after complete decay of background signals [13, 14]. The detection sensitivity of TRF analysis is thus significantly improved compared to traditional fluorescence analysis, making it a fairly suitable technique for the detection of substances in complex samples [15, 16]. Therefore, TRF analysis has been widely applied in immunoassays, biosensing and bioimaging [17, 18].

Persistent luminescence nanoparticles (PLNPs) are long-lived luminescent materials with excellent long afterglow luminescence after ceasing excitation [19]. PLNPs can store energy from excitation sources and slow release it in the forms of light radiation. Compared to other long-lived luminescent materials, PLNPs exhibit many outstanding characteristics: (i) readily available and reusable; (ii) good biocompatibility; and (iii) low toxicity [20, 21]. As a branch of PLNPs, persistent luminescence nanorods (PLNRs) have larger sizes and more binding sites for acceptor. The growth direction of doping elements and host structures are designed to get nanorods with certain length, width, and the ratios of length to width, leading to adjustable characteristic bands of nanorods. Therefore, larger Stokes shifts in nanorods are obtained due to the effects of different dimensional spatial quantum confinement [22, 23].

With the ability to efficiently convert photon energy into heat energy, polydopamine nanoparticles (PDA NPs) have been widely utilized in photothermal therapy as a worthy photothermal reagent [24]. In the present study, a novel PDA-mediated ZnGeO:Mn probe is developed through mixing ZnGeO:Mn PLNRs and PDA NPs for HSA detection. This proposed PDA-mediated ZnGeO:Mn probe exhibits good analysis performance for urinary HSA, which provides a novel method for kidney disease diagnosis. To the best of our knowledge, it is the first time that a TRF probe platform is designed and applied to the HSA detection.

Experimental

Materials and instruments

All reagents and chemicals were analytical grade and used without further purification. $Zn(NO_3)_2{\cdot}6H_2O$, GeO_2, $Mn(NO_3)_2{\cdot}6H_2O$, $NH_3{\cdot}H_2O$ (28 wt%), and dopamine hydrochloride were obtained from Aladdin Bio-Chem Technology Co., Ltd. (Shanghai, China, https://www.aladdin-e.com). $MgCl_2$, Na_2SO_4, $(NH_4)_2SO_4$, CH_3COOK, NaOH, HNO_3, H_3PO_4, acetic acid, boric acid, uric acid, creatinine, and urea were purchased from Sinopharm Chemical Reagent Co., Ltd. (Shanghai, China, http://www.reagent.com.cn). Human serum albumin, casein, transferrin, myoglobin, immunoglobulins (IgG), lactoferrin, lysozyme, and trypsin were obtained from Sigma-Aldrich (Milwaukee, WI, USA, https://www.sigmaaldrich.cn). Ultrapure water was used through the whole experiment.

The TRF measurements and UV–vis absorption spectra were measured on a Spectra Max M5e (Molecular Devices Co. Ltd, USA). The emission delay curves were conducted on a FLS980 steady/transient fluorescence spectrometer (Edinburgh, UK). The morphology of ZnGeO:Mn PLNRs was characterized via a Tecnai G2F20 STWIN (200 kV) transmission electron microscope (FEI, USA). The X-ray photoelectron spectrometer (XPS) characterization of ZnGeO:Mn PLNRs was carried out on a Thermo Scientific™ K-Alpha™+ spectrometer equipped with a monochromatic Al Kα X-ray source (1486.6 eV) operating at 100 W.

TRF detection of HSA with PDA-mediated ZnGeO:Mn probe

ZnGeO:Mn PLNRs and PDA NPs were prepared by the reported methods with minor modification [25, 26] and the preparation process were described in detail in the Supporting Information. PDA NPs and ZnGeO:Mn PLNRs with 3.5 times the mass ratio were added to a BR buffer of pH 5.0 to prepare PDA-mediated ZnGeO:Mn probe. Ninety microliters of PDA-mediated ZnGeO:Mn solution and 10 μL of HSA solution (1–1000 ng mL^{-1}, prepared in a BR buffer of pH 5.0) were mixed in a black 96-well plate with 10-min vibration. Sample was tested in triplicate. Under excitation of 250 nm, the TRF intensity at 540 nm was recorded with delay time of 100 μs and integration time of 1000 μs. The fluorescence quenching efficiency (q) was calculated from the formula of $q = 1 - F/F_0$, in which F and F_0 refer to TRF intensity of PDA-mediated ZnGeO:Mn after and before the addition of HSA, respectively.

Real sample analysis

Urine samples were provided by the Wuxi People's Hospital, which were acquired from healthy volunteers and diabetic patients (the study has been approved by the ethics committee and the number of approval protocol is YL202115). Samples were spiked before filtrating through a 0.45-μm filter membrane and 100-fold diluting with BR (pH 5.0). The spiking concentrations are determined by the range of albumin content in the actual samples from healthy volunteers and diabetic patients [27, 28]. The quantitative analysis of urine samples were performed under the same conditions as HSA standard solutions, and the results were compared with

those obtained by commercialized turbidimetric inhibition immunoassay kits.

Results and discussion

Mechanism of HSA detection

The successful preparation of ZnGeO:Mn PLNRs is proved through high-resolution transmission electron microscopy (HRTEM) and XPS (Fig. S1 and Fig. S2). The obtained ZnGeO:Mn PLNRs show a relatively narrow absorption at 240 nm in the deep ultraviolet region (Fig. 1A, line a). The excitation and emission maxima of ZnGeO:Mn PLNRs in the fluorescence spectra are 250 and 540 nm, respectively (Fig. 1A, line b and c). Figure 1B illustrates the fluorescence decay profiles of ZnGeO:Mn PLNRs, and its lifetime is deduced to be 13.52 ms through a two-exponential function. The TRF intensity of ZnGeO:Mn PLNRs under 0–2.0 mol L^{-1} NaCl is monitored, and virtually no fluctuation is observed even at a high ionic strength (Fig. S3A). The fluorescence stability of ZnGeO:Mn PLNRs is also investigated by continuously detecting the TRF intensity for 1 h, and results indicate that the fluorescence is extremely stable (Fig. S3B).

Initial experiments indicate that the fluorescence of ZnGeO:Mn PLNRs can be quenched by the addition of PDA NPs, and quenched more after further addition of HSA (Fig. 1A, line d and e). PDA NPs shows a main absorption peak at 250 nm (Fig. 1A, line f), which is overlap well with the excitation spectra of ZnGeO:Mn PLNRs. Hence, PDA NPs shield the excitation light of ZnGeO:Mn PLNRs and the fluorescence quenching of ZnGeO:Mn PLNRs is caused by inner filter effect. We assume that the addition of HSA enhances the inner filter effect through increasing the absorption of PDA NPs to the excitation light at 250 nm. However, the absorption of PDA NPs at 250 nm has no significate changes after mixing with different concentrations of HSA (Fig. 2A), indicating that HSA have no influence in the inner filter effect between ZnGeO:Mn PLNRs and PDA NPs.

We further suppose that the fluorescence quenching might be attributed to the interaction between HSA and ZnGeO:Mn PLNRs. The TRF intensity of ZnGeO:Mn PLNRs under HSA is presented as pentagon points and corresponding

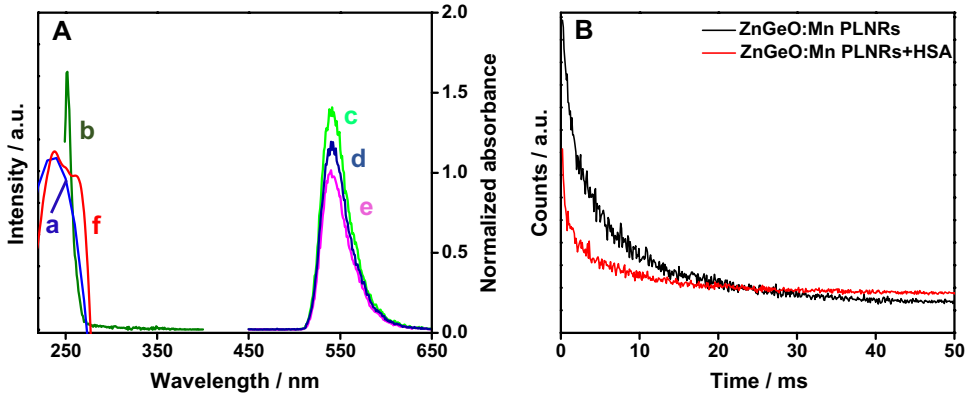

Fig. 1 **A** UV–vis absorption spectra of ZnGeO:Mn PLNRs (a) and PDA NPs (f), fluorescence excitation spectra (λem = 540 nm, b), and fluorescence emission spectra (λex = 250 nm, c) of ZnGeO:Mn PLNRs, fluorescence emission spectra of PDA-mediated ZnGeO:Mn probe in absence (d) and presence (e) of 5 ng mL^{-1} HSA. **B** Luminescence decay curves of ZnGeO:Mn PLNRs in absence and presence of 50 ng mL^{-1} HSA

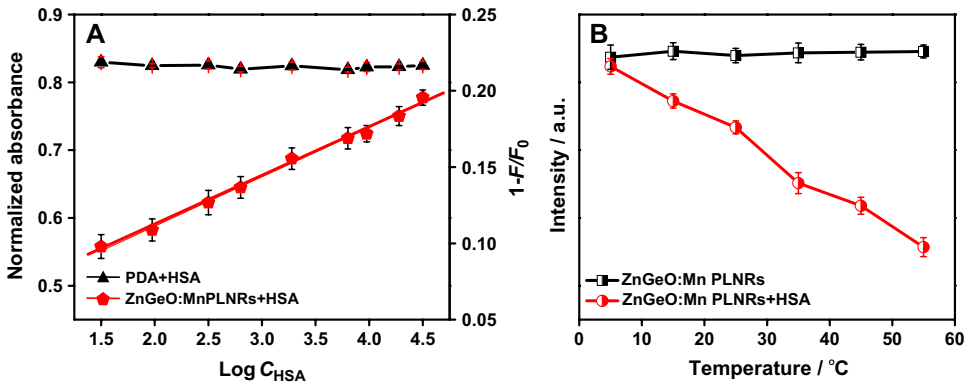

Fig. 2 **A** The absorption at 250 nm of PDA NPs and the fluorescence quenching efficiency of ZnGeO:Mn PLNRs under the addition of HSA. **B** Fluorescence intensity of ZnGeO:Mn PLNRs at 540 nm in absence and presence of 5 ng mL^{-1} HSA under different temperatures

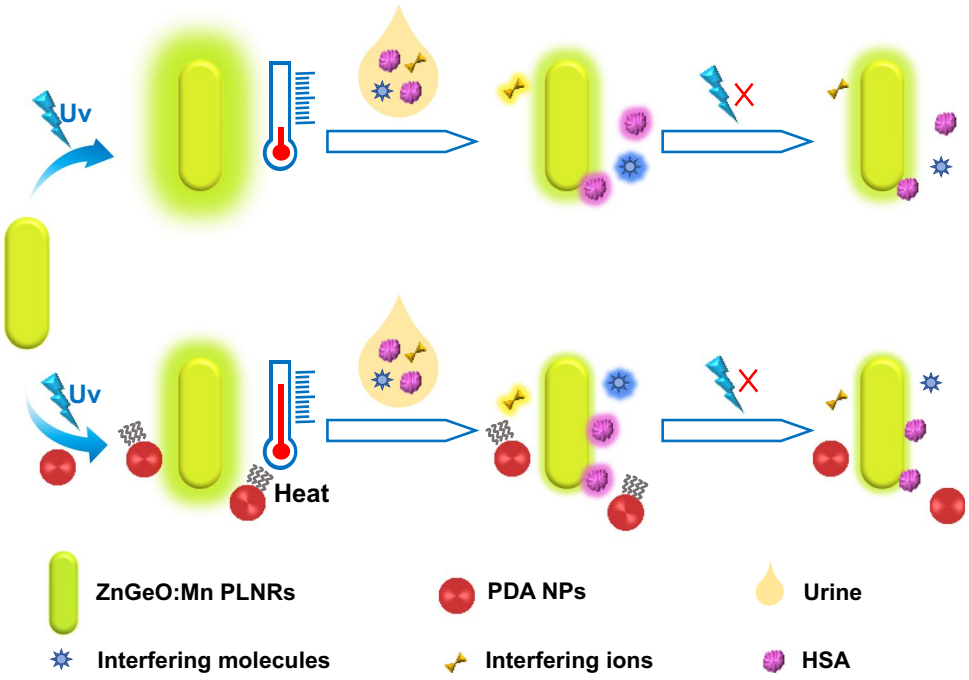

Scheme 1 Schematic illustration of detection mechanism for HSA by the PDA-mediated ZnGeO:Mn probe

lines in Fig. 2A. It can be seen that the fluorescence quenching efficiency increases with HSA concentration. Because the maximum absorption peak of HSA is at 280 nm, the internal filtration effect between HSA and ZnGeO:Mn PLNRs can be excluded. A Stern–Volmer plot is explored to study the quenching mechanism. As shown in Fig. S4, the plot of F_0/F versus HSA concentration fits the conventional Stern–Volmer equation ($F_0/F = 0.0951C_{HSA} + 0.998$, R = 0.996) over the concentration range of 0.1–2 μg mL^{-1}. This result indicates that the dynamic quenching is involved in ZnGeO:Mn PLNRs and HSA.

The quenching mechanism can be further verified by measuring the fluorescence lifetime of ZnGeO:Mn PLNRs before and after adding HSA of 50 ng mL^{-1}, respectively (Fig. 1B). The lifetime of ZnGeO:Mn PLNRs shorten from 13.52 ms to 11.16 ms in the presence of HSA, proving the dynamic quenching between ZnGeO:Mn PLNRs and HSA [29].

The effect of temperature on TRF quenching of ZnGeO:Mn PLNRs is carried out to further confirm the mechanism of dynamic quenching. As illustrated in Fig. 2B, stable fluorescence signals of ZnGeO:Mn PLNRs are obtained with rising temperature and the emission gradually decreases range from 5 to 55 °C upon the addition of 5 ng mL^{-1} HSA. Therefore, the quenching mechanism of the probe is a typical collisional quenching process between ZnGeO:Mn PLNRs and HSA.

The PDA-mediated ZnGeO:Mn probe is developed by simply adding PDA NPs to ZnGeO:Mn PLNRs aqueous solution and vibrating for 10 min (Scheme 1). Anisotropic ZnGeO:Mn PLNRs are used as a TRF agent and possess long luminescence time, which fluorescence intensity decrease upon the addition of HSA in a certain concentration range due to dynamic quenching mechanism. According to the plot of fluorescence quenching efficiency (q) and the logarithm of HSA concentration (0.03–30 μg mL^{-1}) without PDA NPs (Fig. 2A), a regression equation of $q = 0.0324 \log C_{HSA} + 0.046$ (R = 0.997) is obtained with a detection limit of 10 ng mL^{-1}. After the disappearance of excitation light, ZnGeO:Mn PLNRs can continue to glow and the autofluorescence of coexisted contents decays rapidly. Due to the excellent photo-thermal effect of PDA NPs, the solution temperature increases under the light, leading to the increase of collision and then fluorescence quenching between ZnGeO:Mn PLNRs and HSA. Therefore, ZnGeO:Mn PLNRs show better detection performance in the presence of PDA NPs.

HSA determination

According to the optimized conditions (Fig. S5), a PDA: ZnGeO:Mn concentration ratio of 3.5:1, pH of 5.0, and an incubation time of 10 min are used to detect HSA in subsequent experiments. To explore the analysis performance of PDA-mediated ZnGeO:Mn probe to HSA, the TRF intensity (Ex = 250 nm, Em = 540 nm) of PDA-mediated ZnGeO:Mn probe are recorded after mixing with HSA solutions of different concentrations. Experimental results show that TRF intensity decrease upon the introduction of HSA. As shown in Fig. 3A, the fluorescence quenching efficiency (q) is linearly proportional to the logarithm of HSA concentration in the range of 0.1–100 ng mL^{-1},

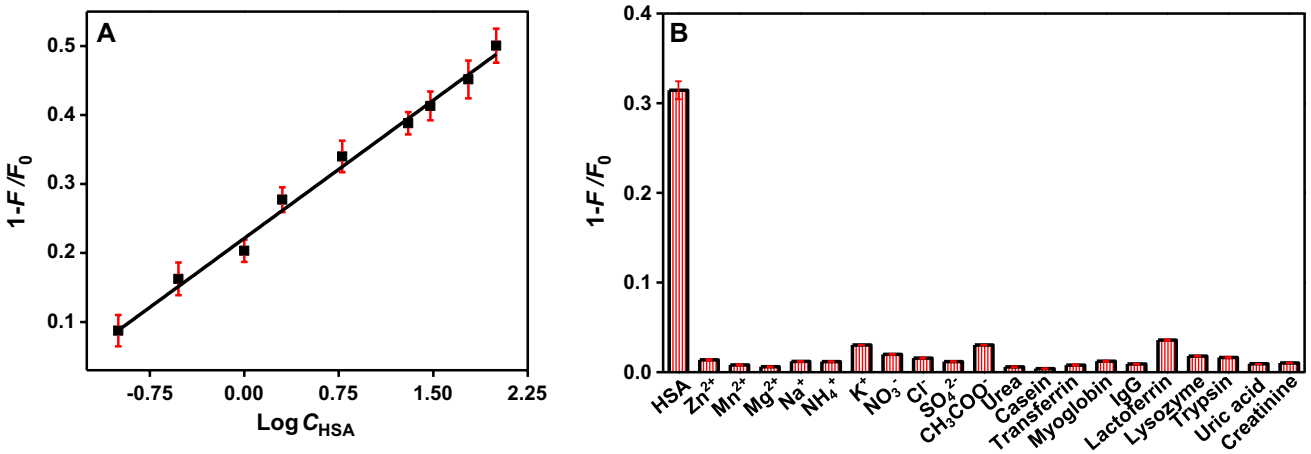

Fig. 3 **A** Linear plot of $1-F/F_0$ vs Log C_{HSA} in the concentration ranges of 0.1–100 ng mL^{-1}. **B** Fluorescence response of the proposed probe toward various ions and biomolecules (the concentrations of HSA, ions, other proteins, urea, uric acid, and creatinine are 5 ng mL^{-1}, 20 μg mL^{-1}, 2 ng mL^{-1}, 40 μg mL^{-1}, 4 μg mL^{-1}, and 4 μg mL^{-1} respectively)

with a regression equation of $q = 0.133 \log C_{HSA} + 0.221$ ($R = 0.994$). The detection limit to HSA is deduced from the ratio of triple standard deviation of blank signal to the slope of calibration plot ($3\sigma/s$, $n = 11$). With the help of PDA NPs, the detection limit of PDA-mediated ZnGeO:Mn probe reduce from 10 ng mL^{-1} to 36 pg mL^{-1}, and the sensitivity increase two orders of magnitude.

Table 1 compares the performance of PDA-mediated ZnGeO:Mn probe with other fluorescent HSA sensors in terms of linear range and limit of detection. It can be seen that PDA-mediated ZnGeO:Mn probe developed in this study exhibit the highest sensitivity.

To investigate the selectivity of PDA-mediated ZnGeO:Mn probe toward HSA, potential interfering substances including metal cations (Zn^{2+}, Mn^{2+}, Mg^{2+}, Na^+, NH_4^+, K^+), anions (NO_3^-, Cl^-, SO_4^{2-}, CH_3COO^-), proteins (casein, transferrin, myoglobin, IgG, lactoferrin, lysozyme, trypsin), urea, uric acid, and creatinine are added to PDA-mediated ZnGeO:Mn solution. The concentrations of ions, proteins, urea, uric acid, and creatinine are 20 μg mL^{-1}, 2 ng mL^{-1}, 40 μg mL^{-1}, 4 μg mL^{-1}, and 4 μg mL^{-1} respectively. As verified in Fig. 3B, there is no significant fluorescence quenching in presence of interference, demonstrating the selectivity of this probe on HSA.

Detection of urinary albumin

Nephropathy as a complication of diabetes, about 4.9–10% of patients with diabetes have proteinuria [35]. It is extremely necessary to detect albumin in urine, due to its important role in early diagnosis of diabetic nephropathy. For the practical application of PDA-mediated ZnGeO:Mn probe in HSA determination, we estimate the albumin levels in NIM-RM3651 solution (1 mL of solution contains 5 mg of powder) and human urine samples from TRF intensity values using the calibration plot. The HSA contents in the urine samples are also detected by the turbidimetric inhibition immunoassay.

Table 2 illustrates the determination results from healthy volunteers and diabetic. The spiked recoveries are in the range of 96.2–106.0%, indicating the potential feasibility of this HSA probe. The results obtained by the present PDA-mediated ZnGeO:Mn probe are in reasonable agreement with those obtained by the turbidimetric inhibition immunoassay, demonstrating the accuracy of the present probe. The results indicated that one of the volunteers with diabetes has higher HSA levels than normal level, which is consistent with clinical results.

Table 1 Comparisons on the performances of this probe with various fluorescent sensors for HSA detection

Fluorescence sensor	Linear range (μg.mL^{-1})	LOD (μg.mL^{-1})	Refs
Urea derivative containing anthracene and naphthalene	2.0×10–8.0×10^2	5.0	[30]
Berberine analogues with hydrophobic substitutions	4.0–6.6×10	1.1	[31]
Graphene oxide-mediated fluorescence quenching aptasensor	1.0×10^{-1}–6.0×10^2	5.0×10^{-2}	[32]
Ionic liquid decorated AIE luminogen	2.0×10^{-2}–1.0×10	7.0×10^{-3}	[33]
The push–pull dyes based sodium sulfonate probe	1.0–3.6×10^2	3.0×10^{-1}	[34]
PDA-mediated ZnGeO:Mn probe	1.0×10^{-4}–1.0×10^{-1}	3.6×10^{-5}	This study

Table 2 The determination of HSA contents in human urine samples ($n=3$, at 95% confidence level)

Sample	PDA-mediated ZnGeO:Mn probe				Turbidimetric inhibition immunoassay	
	Spiked (μg mL^{-1})	Found (μg mL^{-1})	Recovery (%)		Found (μg mL^{-1})	Recovery (%)
NIM-RM3651	0	4.54 ± 0.27	106.0 ± 4.2		4.2 ± 0.3	98.0 ± 3.3
Urine 1 (Healthy)	0	3.50 ± 0.12			3.6 ± 0.2	
	2	5.42 ± 0.22	98.5 ± 2.3		5.3 ± 0.4	94.6 ± 2.9
	5	8.18 ± 0.13	96.2 ± 1.4		8.3 ± 0.6	96.5 ± 1.3
	8	12.15 ± 0.24	105.7 ± 1.2		11.9 ± 0.8	102.6 ± 4.6
Urine 2 (Healthy)	0	1.72 ± 0.13			1.7 ± 0.2	
	2	3.75 ± 0.09	100.8 ± 3.1		3.9 ± 0.2	105.4 ± 4.1
	5	6.56 ± 0.11	97.6 ± 2.8		6.4 ± 0.4	95.5 ± 3.2
	8	9.89 ± 0.23	101.7 ± 2.6		9.8 ± 0.3	101.0 ± 2.4
Urine 3 (Healthy)	0	1.19 ± 0.22			1.1 ± 0.1	
	2	3.13 ± 0.31	98.1 ± 2.2		3.3 ± 0.1	106.5 ± 4.6
	5	6.36 ± 0.22	102.7 ± 1.2		6.0 ± 0.5	98.4 ± 2.8
	8	9.42 ± 0.45	102.5 ± 1.6		8.8 ± 0.7	96.7 ± 3.5
Urine 4 (Diabetic)	0	5.29 ± 0.62			5.4 ± 0.4	
	2	7.56 ± 0.51	103.7 ± 2.4		7.7 ± 0.2	104.1 ± 2.1
	5	10.87 ± 0.42	105.6 ± 3.0		10.7 ± 0.8	102.9 ± 1.9
	8	13.54 ± 0.76	101.9 ± 1.9		12.9 ± 1.0	96.3 ± 2.5
Urine 5 (Diabetic)	0	1.31 ± 0.32			1.4 ± 0.3	
	2	3.44 ± 0.43	103.9 ± 1.1		3.6 ± 0.1	105.9 ± 1.1
	5	6.12 ± 0.52	97.0 ± 2.8		6.0 ± 0.3	93.8 ± 2.0
	8	9.24 ± 0.61	99.2 ± 3.6		9.1 ± 0.7	96.8 ± 3.4
Urine 6 (Diabetic)	0	49.21 ± 0.73			49.5 ± 1.3	
	10	60.31 ± 1.59	101.9 ± 1.0		57.2 ± 2.4	96.1 ± 2.8
	30	80.08 ± 0.92	101.1 ± 2.6		77.5 ± 3.5	97.5 ± 3.6
	50	97.99 ± 0.76	98.8 ± 3.5		96.2 ± 1.7	96.7 ± 4.2

Conclusions

We have established a TRF probe for HSA analysis based on PDA-mediated ZnGeO:Mn via simply mixing of label-free ZnGeO:Mn PLNRs and PDA NPs. The specific collision between HSA and ZnGeO:Mn PLNRs induce the fluorescence quenching of ZnGeO:Mn PLNRs. The large surface area and outstanding long afterglow luminescence of ZnGeO:Mn PLNRs provide the basis for high sensitive TRF detection of HSA. The incorporation of PDA NPs can increase the ambient temperature of solution and promote the dynamic quenching of ZnGeO:Mn PLNRs, further improving the detection sensitivity for HSA. Compared to the reported method, the developed PDA-mediated ZnGeO:Mn probe is much simpler and exhibit higher sensitivity in HSA quantifying, allowing successful determination of albumin in human urine. In other words, the PDA-mediated ZnGeO:Mn probe developed in this study can be employed for early screening of diabetic nephropathy. Taking advantage of the easy access and adjustment to PLNRs, we believe that the detection of other biomolecules can also be achieved by modifying functional groups and ligands on ZnGeO:Mn PLNRs. However, owing to the strong scattering and absorption coefficient of urine to the UV excitation light, the excitation efficiency and signal-to-noise ratio is reduced. Visible light excitable PLNPs and near-infrared excitable PLNPs are new options for future applications. In addition, a POCT (point-of-care testing) system based on this simple and sensitive TRF probe should be developed to facilitate the practical application.

Supplementary Information The online version contains supplementary material available at https://doi.org/10.1007/s00604-021-05097-1.

Acknowledgements The authors appreciate the financial support from the Wuxi Science and Technology Development Foundation (N20202038).

Declarations

Conflict of interest The authors declare that they have no known competing financial interests or personal relationships that could have appeared to influence the work reported in this paper.

References

1. Kumar CV, Buranaprapuk A, Opiteck GJ, Moyer MB, Jockusch S, Turro NJ (1998) Photochemical protease: site-specific photocleavage of hen egg lysozyme and bovine serum albumin. Proc Natl Acad Sci U S A 95(18):10361–10366
2. He XM, Carter DC (1992) Atomic structure and chemistry of human serum albumin. Nature 358(6383):209–215
3. Curry S, Mandelkow H, Brick P, Franks N (1998) Crystal structure of human serum albumin complexed with fatty acid reveals an asymmetric distribution of binding sites. Nat Struct Biol 5(9):827–835
4. Dey G, Gaur P, Giri R, Ghosh S (2016) Optical signaling in biofluids: a nondenaturing photostable molecular probe for serum albumins. Chem Commun 52(9):1887–1890
5. de Zeeuw D, Parving HH, Henning RH (2006) Microalbuminuria as an early marker for cardiovascular disease. J Am Soc Nephrol 17(8):2100–2105
6. Sugimori H, Tomoda F, Koike T, Kurosaki H, Masutani T, Ohara M, Kagitani S, Inoue H (2013) Increased blood viscosity is associated with reduced renal function and elevated urinary albumin excretion in essential hypertensives without chronic kidney disease. Hypertens Res 36(3):247–251
7. Hui S, Zhou N, Ying SF (2010) Determination of free bilirubin and its binding capacity by HSA using a microfluidic chip-capillary electrophoresis device with a multi-segment circular-ferrofluid-driven micromixing injection. Electrophoresis 31(18):3061–3069
8. Lin ZH, Chen IC, Chang HT (2011) Detection of human serum albumin through surface-enhanced Raman scattering using gold "pearl necklace" nanomaterials as substrates. Chem Commun 47(25):7116–7118
9. Snozek CLH, Saenger AK, Greipp PR, Bryant SC, Kyle RA, Rajkumar SV, Katzmann JA (2007) Comparison of bromcresol green and agarose protein electrophoresis for quantitation of serum albumin in multiple myeloma. Clin Chem 53(6):1099–1103
10. Suzuki Y, Yokoyama K (2005) Design and synthesis of intramolecular charge transfer-based fluorescent reagents for the highly-sensitive detection of proteins. J Am Chem Soc 127(50):17799–17802
11. Duan R, Wang B, Zhang T, Zhang Z, Xu S, Chen Z, Lou X, Xia F (2014) Sensitive and bidirectional detection of urine telomerase based on the four detection-color states of difunctional gold nanoparticle probe. Anal Chem 86(19):9781–9785
12. Gatterdam V, Frutiger A, Stengele KP, Heindl D, Lubbers T, Voros J, Fattinger C (2017) Focal molography is a new method for the in situ analysis of molecular interactions in biological samples. Nat Nanotechnol 12(11):1089–1095
13. Suhling K, French PMW, Phillips D (2005) Time-resolved fluorescence microscopy. Photoch Photobio Sci 4(1):13–22
14. Laursen BW, Bogh SA, Sorensen TJ (2020) Long fluorescence lifetime triangulenium dyes in imaging and fluorescence polarization assay. Method Enzymol 640:249–265
15. Yuan J, Wang G (2006) Lanthanide-based luminescence probes and time-resolved luminescence bioassays. Trends Analyt Chem 25(5):490–500
16. Zheng W, Tu D, Huang P, Zhou S, Chen Z, Chen X (2015) Time-resolved luminescent biosensing based on inorganic lanthanide-doped nanoprobes. Chem Commun 51(20):4129–4143
17. Deng Q, Zhu Z, Shu X (2020) Auto-phase-locked time-resolved luminescence detection: principles, applications, and prospects. Front Chem 8:562–566
18. Ma Q, Wang J, Li Z, Lv X, Liang L, Yuan Q (2019) Recent progress in time-resolved biosensing and bioimaging based on lanthanide-doped nanoparticles. Small 15:1804969
19. Zhang KY, Yu Q, Wei H, Liu S, Zhao Q, Huang W (2018) Long-lived emissive probes for time-resolved photoluminescence bioimaging and biosensing. Chem Rev 118(4):1770–1839
20. Liang L, Chen N, Jia Y, Ma Q, Wang J, Yuan Q, Tan W (2019) Recent progress in engineering near-infrared persistent luminescence nanoprobes for time-resolved biosensing/bioimaging. Nano Res 12(6):1279–1292
21. Zhao X, Chen LJ, Zhao KC, Liu YS, Liu JL, Yan XP (2019) Autofluorescence-free chemo/biosensing in complex matrixes based on persistent luminescence nanoparticles. Trends Analyt Chem 118:65–72

22. Wang J, Ma Q, Zheng W, Liu H, Yin C, Wang F, Chen X, Yuan Q, Tan W (2017) One-dimensional luminous nanorods featuring tunable persistent luminescence for autofluorescence-free biosensing. ACS Nano 11:8185–8191
23. Wu S, Li Y, Ding W, Xu L, Ma Y, Zhang L (2020) Recent advances of persistent luminescence nanoparticles in bioapplications. Nanomicro Lett 12(1):1–26
24. Liu Y, Ai K, Liu J, Deng M, He Y, Lu L (2013) Dopamine-melanin colloidal nanospheres: an efficient near-infrared photothermal therapeutic agent for in vivo cancer therapy. Adv Mater 25(9):1353–1359
25. Wang Y, Li Z, Lin Q, Wei Y, Wang J, Li Y, Yang R, Yuan Q (2019) Highly sensitive detection of bladder cancer-related miRNA in urine using time-gated luminescent biochip. Acs Sens 4(8):2124–2130
26. Shi L, Shao J, Jing X, Zheng W, Liu H, Zhao Y (2020) Autoluminescence-free dual tumor marker biosensing by persistent luminescence nanostructures. Acs Sustain Chem Eng 8:686–694
27. Marrack JR, Johns RGS (1950) Albumin in normal urine. Biochemical 47:3
28. Davies AG, Price DA, Postlethwaite RJ, Fielding BA (1985) Urine albumin excretion in diabetics. Lancet 8426(1):466–467
29. Liu Y, Wang Y, Jiang K, Sun S, Qian S, Wu Q, Lin H (2020) A persistent luminescence-based label-free probe for the ultrasensitive detection of hemoglobin in human serum. Talanta 206:120206
30. Halder S, Samanta S, Das G (2019) Exploring the potential of a urea derivative: an AIE-luminogen and its interaction with human serum albumin in aqueous medium. Analyst 144(8):2696–2703
31. Nayim S, Jana GC, Aktara MN, Khatun M, Das S, Islam MM, Jha PK, Hossain M (2019) Berberine derivatives as heteroatom induced hydrophobic sensor: an analytical approach for the selective and sensitive fluorometric detection and discrimination of serum albumins. Anal Chim Acta 1065:124–133
32. Chawjiraphan W, Apiwat C, Segkhoonthod K, Treerattrakoon K, Pinpradup P, Sathirapongsasuti N, Pongprayoon P, Luksirikul P, Isarankura-Na-Ayudhya P, Japrung D (2020) Albuminuria detection using graphene oxide-me diate d fluorescence quenching aptasensor. Methodsx 7:101114
33. Gao L, Lin X, Chen X (2020) Ionic liquid decorated AIE luminogen for selective detection of HSA in biofluids and early disease screening. Talanta 212:120763
34. Park J, Kim Y (2019) Colloidal fluorophore aggregates for the selective detection of albumins in solution and on electrophoresis gels. ChemBioChem 20(3):350–354
35. Jain V, Sharma A, Agrawal N, Dhawale RG (2020) Estimation of urine albumin to creatinine ratio and its correlation with the complications in diabetes mellitus. J Assoc Physicians India 68:49–53

Publisher's note Springer Nature remains neutral with regard to jurisdictional claims in published maps and institutional affiliations.